

New Topologies in Pentanuclear Nickel/Oximate Clusters: Structural and Magnetic Characterization

Jordi Esteban,^{*,†} Mercè Font-Bardia,^{‡,§} José Sánchez Costa,^{†,⊥} Simon J. Teat,^{||} and Albert Escuer^{*,†}

[†]Departament de Química Inorgànica, Universitat de Barcelona, Avinguda Diagonal 645, 08028 Barcelona, Spain

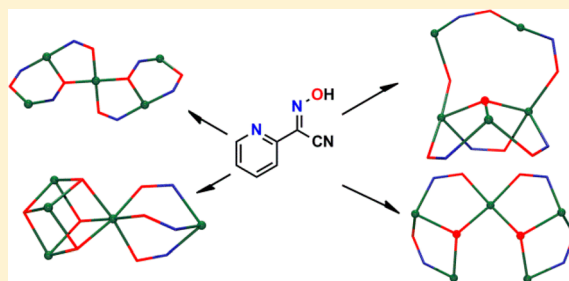
[‡]Departament de Mineralogia, Cristal·lografia i Dipòsits Minerals, Universitat de Barcelona, Martí Franquès s/n, 08028 Barcelona, Spain

[§]Unitat de Difracció de R-X. Centre Científic i Tecnològic de la Universitat de Barcelona (CCiTUB). Universitat de Barcelona, Solé i Sabarís 1–3, 08028 Barcelona, Spain

^{||}Advanced Light Source, Lawrence Berkeley National Laboratory, 1 Cyclotron Road, Berkeley, California 94720, United States

S Supporting Information

ABSTRACT: In the present work, five new Ni₅ clusters employing the versatile 2-pyridylcyanoxime ligand have been synthesized and chemically, structurally, and magnetically characterized. The crystallographic examination of these Ni₅ clusters together with those already published in the literature, giving a total number of 14 complexes, exhibiting up to 8 different topologies for which the relationship between topology, reaction conditions and magnetic response has been analyzed. DC magnetic measurements were carried in the 300–2 K range for the new complexes and the analysis of the experimental data revealed an antiferromagnetic response for the oximate mediated interactions with a variety of ground states ($S = 0, 1, 3$) as function of the cluster topology.



INTRODUCTION

Chemistry of 3D metallic clusters is a continuously growing research field due its intrinsic interest in coordination chemistry and the relevance in research fields, such as bioinorganic chemistry¹ or molecular nanomagnetism.²

Rational design of clusters and tailoring of the derived properties has been reached in some cases employing rigid ligands and the “designed assembly” approach to obtain polygons or polyhedral compounds by Lehn,³ Fujita,⁴ and other authors.⁵ However, most of the reported cluster chemistry is obtained following the named “serendipitous assembly”, consisting of one-pot reactions of the adequate ligands, pH, solvents, and metallic salts. This approach has proven to be extremely successful, but fundamental aspects, such as nuclearity, topology, or the derived properties, become largely unpredictable, and only the analysis of the properties of large series of complexes can give an approach to improve future synthetic work.⁶

2-Pyridyloximes have been widely employed in cluster chemistry and molecular magnetism studies along the last years because of their ability to coordinate several metallic centers, to stabilize discrete clusters and their efficient behavior as magnetic coupler.⁷ These ligands are also attractive to experimental coordination chemists by their apparently unpredictable coordinative properties, which are reflected in the large number of nuclearities and topologies characterized to date, which are often modified even as response to small

changes in the reaction conditions. As example, nickel clusters of 2-pyridyloximes show practically all nuclearities between Ni₃ and Ni₁₄ (except for Ni₁₁)⁸ and a surprising variety of topologies considering that a CCDC database search results in 78 entries, reflecting the specially “serendipitous” character of this family of ligands.

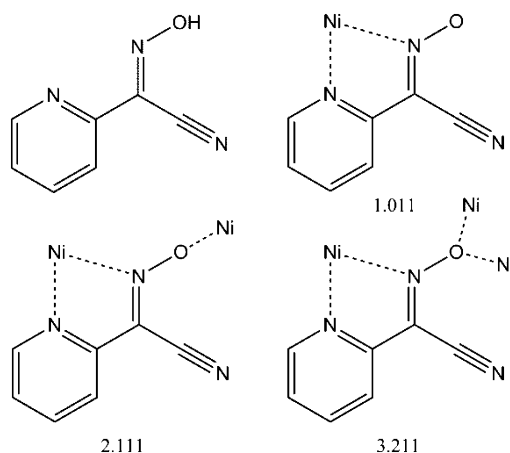
Given the fact that the chances of identifying new types of coordination clusters with improved or novel properties can be increased by the development of new reaction systems with suitable metal precursors and ligands, and following our work in this field, we have chosen the 2-pyridylcyanoxime ligand, pyC{CN}NOH, Scheme 1, to continue the exploration of the synthesis of oximate metallic clusters.

This choice has been made on the basis of the unique properties of pyC{CN}NOH ligand related to the cyano substituent on the vicinal C-atom to the oximate function, which gives a much more acidic oxime (3–5 units of p*K*_a) respect to ligands with other substituents.⁷ PyC{CN}NOH ligand has proven to be a valid ligand to synthesize complexes with unusual topologies (as we have reported in previous copper,⁹ nickel,^{8a,10} and manganese¹¹ studies), and in contrast with all the other members of this family of ligands, we have observed its specific tendency to generate μ₃-OR/oximate triangular-based complexes and clusters with Ni₃ and Ni₅

Received: January 9, 2014

Published: March 4, 2014

Scheme 1. PyC{CN}NOH Ligand and Coordination Modes for pyC{CN}NO⁻ Found in Compounds 1–5 (in Harris Notation¹²)



nuclearity.^{8a,10} Notably, 7 of the 14 compounds obtained with this ligand in Ni^{II} chemistry, including the five new clusters presented in this paper, exhibit the Ni₅ nuclearity.^{8a,10}

In this Article, we report the characterization of series of pentanuclear nickel clusters obtained by reaction of Ni^{II} salts and pyC{CN}NOH ligand with formula (NEt₄)-[Ni₅(OH)₂(Ph₂CHCOO)₅(pyC{CN}NO)₄(H₂O)] (1), [Ni₅Cl₂(pyC{CN}NO)₈(H₂O)₂] (2), [Ni₅Br₃(MeO)₄(pyC{CN}NO)₃(MeOH)₆] (3), [Ni₅(NCS)₂(OH)₂(pyC{CN}NO)₆(H₂O)₃] (4), and [Ni₅(MeO)₂(OH)_{1.5}(pyC{CN}NO)₆(H₂O)_{2.5}(MeOH)](NO₃)_{0.5} (5).

The reported complexes provide several new cores for the Ni₅/2-pyridyloximato system and, therefore, the aim of this work is not only to present the new compounds but to review the different topologies for this nuclearity in the search of some relationship between the structural data, the reaction conditions and the magnetic properties, which can be useful in order to rationalize the “serendipitous” behavior of this kind of ligands.

EXPERIMENTAL SECTION

2-Pyridylacetonitrile and the nickel salts were purchased from Sigma-Aldrich Inc. and used without further purification. Ni(Ph₂CHCOO)₂·xH₂O was synthesized dissolving equimolar quantities (40 mmol) of diphenylbenzoic acid and NaOH in 40 mL of H₂O, filtering, and mixing the final solution with a commercial source of Ni(NO₃)₂·6H₂O (20 mmol) in 20 mL of water. The resulting nickel salt was obtained in good yield (>80%). Samples for analysis were dried to remove the volatile crystallization solvents.

pyC{CN}NOH. The ligand was prepared following a modification of the procedure¹³ reported in the literature: reaction of equimolar ratio of pyCH₂CN, acetic acid, and KNO₂ was set under stirring for two hours in an ice-bath, and then the brown product was filtered and cleaned with abundant water. The ligand was collected as a brown solid in 40% yield.

(NEt₄)[Ni₅(OH)₂(Ph₂CHCOO)₅(pyC{CN}NO)₄(H₂O)]·3CH₂Cl₂·H₂O (1·3CH₂Cl₂·H₂O). PyC{CN}NOH (0.073 g, 0.5 mmol), Ni(Ph₂CHCOO)₂·xH₂O (0.240 g, 0.5 mmol), and NaN(CN)₂ (0.089 g, 1 mmol) were dissolved in 20 mL of dichloromethane together with NEt₃ (0.101 g, 1 mmol). The mixture was stirred for 2 h and then filtered. Crystals were obtained by layering the final solution with 10 mL of hexane. Green bricks adequate for X-ray diffraction appeared a week after. Anal. Calcd for C₁₀₆H₉₇N₁₃Ni₅O₁₈ (1·H₂O): C, 59.65; H, 4.58; N, 8.53%. Found: C, 59.1; H, 4.3; N, 8.7%. Relevant IR bands (cm⁻¹): 3420(br), 2211(w), 1601(s), 1457(s), 1419(m), 1392(m), 1302(w), 1269(w), 1230(m), 1154(w), 1105(w), 1037(w), 781(w), 745(m), 708(m).

[Ni₅Cl₂(pyC{CN}NO)₈(H₂O)₂]·2CH₂Cl₂·H₂O (2·2CH₂Cl₂·H₂O). Twenty mL of CH₂Cl₂ were poured over pyC{CN}NOH (0.073 g, 0.5 mmol), NiCl₂·6H₂O (0.238 g, 1 mmol) and NEt₃ (0.101 g, 1 mmol). The mixture was stirred for a couple of hours, then filtered and finally layered with 10 mL of hexane. Red prismatic crystals were collected after two weeks. Anal. Calcd for C₅₆Cl₂H₃₈N₂₄Ni₅O₁₁ (2·H₂O): C, 42.37; H, 2.41; N, 21.18%. Found: C, 42.4; H, 2.6; N, 20.7%. Relevant IR bands (cm⁻¹): 3425(br), 2217(w), 1601(s), 1460(s), 1426(m), 1399(m), 1302(m), 1266(w), 1221(s), 1155(m), 1107(m), 1061(w), 1037(s), 1007(w), 780(m), 746(w), 709(s).

[Ni₅Br₃(MeO)₄(pyC{CN}NO)₃(MeOH)₆]·1.5MeOH·0.5H₂O (3·1.5MeOH·0.5H₂O). PyC{CN}NOH (0.073 g, 0.5 mmol) was dissolved in 20 mL of MeOH with NiBr₂·xH₂O (0.218 g, 1 mmol) and NEt₃ (0.101 g, 1 mmol). The mixture was stirred for two hours, filtered and left for slow evaporation in an open vial. Dark prismatic crystals adequate for X-ray diffraction were obtained after two weeks. Anal. Calcd for C₃₁Br₃H₄₉N₉Ni₅O_{13.5} (3·0.5H₂O): C, 28.71; H, 3.81;

Table 1. Crystal Data, Data Collection, and Structure Refinement Details for the X-ray Structure Determination of Compounds 1–5

	1	2	3	4	5
formula	C ₁₀₉ H ₁₀₂ Cl ₆ N ₁₃ Ni ₅ O ₁₈	C ₅₈ Cl ₆ H ₄₂ N ₂₄ Ni ₅ O ₁₁	C ₆₅ H ₁₀₄ Br ₆ N ₁₈ Ni ₁₀ O ₃₀	C ₂₁₇ H ₂₀₈ N ₁₀₀ Ni ₂₀ O ₆₂ S ₈	C ₁₉₁ H ₂₁₆ N ₇₄ Ni ₂₀ O ₇₄
fw	2388.19	1575.41	2684.22	6639.51	5906.58
system	monoclinic	monoclinic	trigonal	monoclinic	tetragonal
space group	P2 ₁ /c	P2 ₁ /c	R $\bar{3}$	C2/c	P4 ₂ /n
a (Å)	16.734(2)	15.674(2)	15.210(7)	32.360(2)	34.0083(4)
b (Å)	24.440(3)	14.767(2)	15.210(7)	23.188(1)	34.0083(4)
c (Å)	28.002(3)	18.470(2)	40.38(2)	23.240(1)	12.0595(2)
α (deg)	90	90	90	90	90
β (deg)	112.758(5)	108.501(2)	90	101.395(3)	90
γ (deg)	90	90	120	90	90
V (Å ³)	10561(2)	4054.0(8)	8090(7)	17095(2)	13947.6(3)
Z	4	2	3	2	2
T (K)	100(2)	100(2)	105(2)	293(2)	100(1)
λ(MoK _α) (Å)	0.77490	0.71073	0.71073	0.71073	1.54178
ρ _{calcd} (g·cm ⁻³)	1.502	1.440	1.653	1.290	1.406
μ(MoK _α), mm ⁻¹	1.374	1.403	3.999	1.196	2.120
R	0.0725	0.0335	0.0517	0.0521	0.0684
ωR ²	0.2217	0.0914	0.1441	0.2148	0.2190

N, 9.72%. Found: C, 28.3; H, 3.7; N, 10.0%. Relevant IR bands (cm^{-1}): 3427(br), 2221(w), 1602(m), 1467(s), 1427(m), 1303(w), 1263(w), 1220(m), 1157(w), 1108(m), 1032(w), 1037(m), 779(w), 711(m). Reaction starting from $\text{NiCl}_2 \cdot 6\text{H}_2\text{O}$ gives a product with the same IR spectrum but crystals adequate for diffraction were not obtained and thus the sample will no further discussed.

$[\text{Ni}_5(\text{NCS})_2(\text{pyC}\{\text{CN}\}\text{NO})_6(\text{OH})_2(\text{H}_2\text{O})_3] \cdot 5\text{MeCN} \cdot 4\text{H}_2\text{O}$ (4·5MeCN·4H₂O). $\text{PyC}\{\text{CN}\}\text{NOH}$ (0.073 g, 0.5 mmol) was dissolved in 20 mL of MeCN with $\text{Ni}(\text{SCN})_2$ (0.174 g, 1 mmol), $\text{NaN}(\text{CN})_2$ (0.089 g, 1 mmol), and NEt_3 (0.101 g, 1 mmol). The mixture was stirred for 2 h and then filtered. Crystals were obtained by layering the final solution with 10 mL of diethyl ether. Crystals were collected after a couple of weeks. Anal. Calcd for $\text{C}_{44}\text{H}_{40}\text{N}_{20}\text{Ni}_5\text{O}_{15}\text{S}_2$ (4·4H₂O): C, 36.53; H, 2.78; N, 19.37; S, 4.43%. Found: C, 37.3; H, 2.8; N, 18.9; S, 4.2%. Relevant IR bands (cm^{-1}): 3441(br), 2223(w), 2101(w), 1971(w), 1602(s), 1466(s), 1428(m), 1303(w), 1265(w), 1222(m), 1157(w), 1108(m), 1061(w), 1037(m), 778(w), 712(m).

$[\text{Ni}_5(\text{MeO})_2(\text{OH})_{1.5}(\text{pyC}\{\text{CN}\}\text{NO})_6(\text{H}_2\text{O})_{2.5}(\text{MeOH})](\text{NO}_3)_{0.5} \cdot 2.75\text{MeOH} \cdot 1.25\text{H}_2\text{O}$ (5·2.75MeOH·1.25H₂O). $\text{PyC}\{\text{CN}\}\text{NOH}$ (0.073 g, 0.5 mmol) and $\text{Ni}(\text{NO}_3)_2 \cdot 6\text{H}_2\text{O}$ (0.290 g, 1 mmol) were dissolved in 20 mL of MeOH and NEt_3 (0.101 g, 1 mmol). The mixture was stirred for two hours, filtered and left for slow evaporation in an open vial. Red crystals appeared after a month. Anal. Calcd for $\text{C}_{45}\text{H}_{43}\text{N}_{18.5}\text{Ni}_5\text{O}_{15.75}$ (5·1.25H₂O): C, 38.93; H, 3.12; N, 18.66%. Found: C, 38.2; H, 3.3; N, 18.1%. Relevant IR bands (cm^{-1}): 3397(br), 2222(w), 1602(m), 1465(s), 1427(m), 1384(s), 1302(w), 1266(w), 1226(m), 1157(w), 1109(w), 1062(w), 1036(m), 779(w), 711(m).

Physical Measurements. Magnetic susceptibility measurements were carried out on polycrystalline samples with a MPMS5 Quantum Design susceptometer working in the range 30–300 K under external magnetic field of 0.3 T and under a field of 0.03 T in the 30–2 K range to avoid saturation effects. Diamagnetic corrections were estimated from Pascal Tables. Infrared spectra (4000–400 cm^{-1}) were recorded from KBr pellets on a Bruker IFS-125 FT-IR spectrophotometer.

X-ray Crystallography. Details of crystal data, data collection, and refinement for 1–5 are given in Table 1. Data for compound 1 was measured from dark green crystals at 100 K and $\lambda = 0.7749$ Å using a Bruker APEX II CCD diffractometer on Advanced Light Source beamline 11.3.1 at Lawrence Berkeley National Laboratory.

Collection of data for compound 2, 3, 4, and 5 was made on a Bruker CCD SMART1000, a MAR345 diffractometer with an image plate detector, a Bruker X8 KappaAPEXII diffractometer with a CCD detector and a Bruker-Nonius FR591 Kappa CCD 2000, respectively. All structures were solved by direct methods, using SHELXS computer program¹⁴ and refined by full-matrix least-squares method with SHELXL97 computer program.¹⁵ International Tables of X-ray Crystallography¹⁶ were used to minimize the $\sum w||F_o|^2 - |F_c|^2|^2$ function. Lorentz-polarization, and absorption corrections were made.

For compound 1, $\sin(\theta_{\text{max}}/\lambda)$ is lower than 0.5 (0.4587) because of the relatively low scattering and the small size of the crystals which limited the observed reflections. For complex 2, 2H atoms were located from a difference synthesis and refined with an isotropic temperature factor equal to 1.2 times the equivalent temperature factor of the atoms which are linked and 18H atoms were computed and refined, using a riding model, with an isotropic temperature factor equal to 1.2 times the equivalent temperature factor of the atoms which are linked. 3, 4, 5: all H atoms were computed and refined, using a riding model, with an isotropic temperature factor equal to 1.2 times the equivalent temperature factor of the atom which are linked.

All data can be found in the Supporting Information for this paper in cif format with CCDC numbers 970384–970388. These data can also be obtained free of charge from The Cambridge Crystallographic Data Centre via www.ccdc.cam.ac.uk/data_request/cif.

Plots for publication were generated with ORTEP3 for Windows and plotted with Pov-Ray programs.¹⁷

RESULTS AND DISCUSSION

Description of the Structures. $(\text{NEt}_4)-[\text{Ni}_5(\text{OH})_2(\text{Ph}_2\text{CHCOO})_5(\text{pyC}\{\text{CN}\}\text{NO})_4(\text{H}_2\text{O})] \cdot 3\text{CH}_2\text{Cl}_2 \cdot \text{H}_2\text{O}$ (1·3CH₂Cl₂·H₂O). A view of the core of complex 1 is illustrated in Figure 1. Selected interatomic distances and angles for 1 are

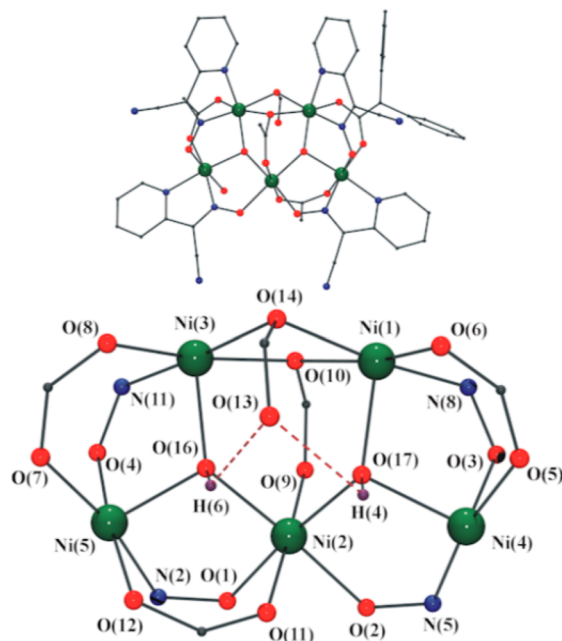


Figure 1. Top: View of complex 1. Phenyl groups have been omitted for clarity except for the $\text{Ph}_2\text{CHCOO}^-$ ligand linked to Ni(3)/Ni(5). Bottom: Partially labeled Pov-Ray plot of complex 1, showing the H bonds involving the μ_3 -OH ligands as red dashed bonds.

listed in Table 2. The core of this anionic compound can be described like two μ_3 -OH centered triangles formed by Ni(1,2,4) and Ni(2,3,5) cations sharing the Ni(2) vertex. Both μ_3 -OH groups are placed slightly out of the plane formed by the three Ni^{II} atoms (0.470 and 0.502 Å, respectively). Ni(1) and Ni(3) are linked together by two $\text{Ph}_2\text{CHCOO}^-$ bridging ligands in 2.20 and 3.21 coordination mode (or η^1, μ -R-COO⁻ and $\eta^2: \eta^1, \mu$ -R-COO⁻ respectively) resulting in a three edge-sharing triangles topology.

Ni(1,2,4) triangle shows Ni(1)···Ni(2), Ni(1)···Ni(4) and Ni(2)···Ni(4) distances of 3.571(2), 3.271(3) and 3.324(2) Å, respectively. The sides of the triangles are defined by one double oximato and syn–syn carboxylato bridge between Ni(1) and Ni(4), one single oximato bridge between Ni(2) and Ni(4) and the $\eta^2: \eta^1, \mu$ -carboxylato ligand between Ni(1) and Ni(2); whereas Ni(2,3,5) triangle exhibits Ni(2)···Ni(3), Ni(2)···Ni(5), and Ni(3)···Ni(5) Ni–Ni distances of 3.606(2), 3.226(2), and 3.290(3) Å, respectively, and is defined by two double oximato/syn–syn carboxylato bridges between Ni(5) and Ni(2,3) and one $\eta^2: \eta^1, \mu$ -carboxylato bridge between Ni(2) and Ni(3). In the inner triangle, the Ni(1)···Ni(3) distance is 3.236(2) Å.

The coordination environment of Ni(2) (the shared vertex) is NiO₆, provided by the two μ_3 -OH groups, two O-oximato bridges, one syn–syn $\text{Ph}_2\text{CHCOO}^-$ ligand and the $\eta^2: \eta^1, \mu$ -diphenylacetate bridge, whereas each remaining nickel centers is linked to one $\text{pyC}\{\text{CN}\}\text{NO}^-$ ligand by their two N atoms exhibiting a NiN₂O₄ environment. All $\text{pyC}\{\text{CN}\}\text{NO}^-$ ligands exhibit the same 2.111 coordination mode.

Table 2. Selected Interatomic Distances (Å) and Angles (deg) for Compound 1

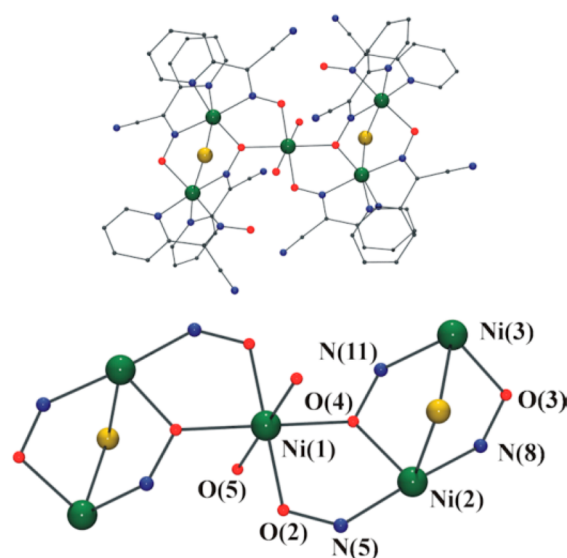
Ni(1)–N(7)	2.07(1)	Ni(1)–N(8)	2.037(9)
Ni(1)–O(6)	2.042(7)	Ni(1)–O(10)	2.172(7)
Ni(1)–O(14)	2.114(7)	Ni(1)–O(17)	2.012(9)
Ni(2)–O(1)	2.038(9)	Ni(2)–O(2)	2.063(9)
Ni(2)–O(9)	2.075(8)	Ni(2)–O(11)	2.10(1)
Ni(2)–O(16)	2.043(7)	Ni(2)–O(17)	2.046(7)
Ni(3)–N(10)	2.10(1)	Ni(3)–N(11)	2.05(1)
Ni(3)–O(8)	2.035(7)	Ni(3)–O(10)	2.117(7)
Ni(3)–O(14)	2.170(7)	Ni(3)–O(16)	1.983(9)
Ni(4)–N(4)	2.08(1)	Ni(4)–N(5)	2.03(1)
Ni(4)–O(3)	2.056(9)	Ni(4)–O(5)	2.028(8)
Ni(4)–O(15)	2.16(1)	Ni(4)–O(17)	2.013(8)
Ni(5)–N(1)	2.06(1)	Ni(5)–N(2)	2.04(1)
Ni(5)–O(4)	2.056(9)	Ni(5)–O(7)	2.041(8)
Ni(5)–O(12)	2.069(9)	Ni(5)–O(16)	2.010(8)
Ni(1)–O(17)–Ni(2)	123.3(4)	Ni(1)–O(17)–Ni(4)	108.7(4)
Ni(2)–O(17)–Ni(4)	110.0(4)	Ni(2)–O(16)–Ni(3)	127.2(4)
Ni(2)–O(16)–Ni(5)	105.5(3)	Ni(3)–O(16)–Ni(5)	111.0(4)
Ni(1)–O(10)–Ni(3)	98.0(3)	Ni(1)–O(14)–Ni(3)	98.1(4)
Ni(1)–N(8)–O(3)–Ni(4)	20(1)	Ni(3)–N(11)–O(4)–Ni(5)	18(1)
Ni(4)–N(5)–O(2)–Ni(2)	4(1)	Ni(5)–N(2)–O(1)–Ni(2)	8(1)

Complex 1 contains three different $\text{Ph}_2\text{CHCOO}^-$ coordination modes: three carboxylates are coordinated in the syn–syn mode, one links three metallic centers in its tridentate 3.21 mode and the last one links two nickel ions in its 2.20 mode. The noncoordinated O(13) atom from the 2.20 $\text{Ph}_2\text{CHCOO}^-$ ligand establishes two strong intramolecular H-bonds with the hydroxo ligands with O(13)⋯O(16) and O(13)⋯O(17) distances of 3.02(1) and 2.904(9) Å, respectively).

Ni–O–Ni bond angles involving the μ_3 -OH group show one large and two smaller angles in each triangle (123.3(4)/110.0(4)/108.7(4)° and 127.2(4)/111.0(4)/105.5(3)°, Table 2). The crystallization water molecule forms two additional intramolecular H bonds with the water molecule bonded to Ni(4) and the O(13) atom. Relevant H-bonds or other intermolecular interactions were not found.

Charge balance is achieved by means of one tetraethylammonium cation, which was the product of the reaction of the triethylamine (employed as base in the synthesis) and the dichloromethane solvent. Reactivity of di- or trialkylamines with dichloromethane in mild conditions was early established^{18a} and the use of triethylamine as base and CH_2Cl_2 as solvent in nickel or manganese chemistry can lead, probably catalyzed by the cation, to a wide variety of products such as Et_4N^+ , Et_2NH_2^+ , or chloro-alkyl derivatives.^{18b,c}

$[\text{Ni}_5\text{Cl}_2(\text{pyC}\{\text{CN}\}\text{NO})_8(\text{H}_2\text{O})_2] \cdot 2\text{CH}_2\text{Cl}_2 \cdot \text{H}_2\text{O}$ (**2**). The centrosymmetric molecule of **2** consists on a central Ni^{II} atom connected to the four peripheral Ni^{II} centers via four oximate bridges and can be described like a distorted bowtie, Figure 2. Selected interatomic distances and angles for **2** are listed in Table 3. The NiO_6 environment of the central Ni(1) atom arises from four O-oximate atoms and two trans water molecules, whereas all peripheral nickel atoms exhibit NiClN_4O environments formed by two $\text{pyC}\{\text{CN}\}\text{NO}^-$ ligands, one bridging chloride atom and one O-oximate donor.

**Figure 2.** Top: View of complex 2. Bottom: Partially labeled Pov-Ray plot of complex 2. All hydrogen atoms have been omitted for clarity.**Table 3. Selected Interatomic Distances (Å) and Angles (deg) for Compound 2**

Ni(1)–O(2)	2.033(2)	Ni(1)–O(4)	2.108(2)
Ni(1)–O(5)	2.038(2)		
Ni(2)–O(4)	2.062(2)	Ni(2)–N(7)	2.075(2)
Ni(2)–N(4)	2.058(2)	Ni(2)–N(8)	2.053(2)
Ni(2)–N(5)	2.030(3)	Ni(2)–Cl(1)	2.413(1)
Ni(3)–O(3)	2.076(2)	Ni(3)–N(10)	2.073(2)
Ni(3)–N(1)	2.049(3)	Ni(3)–N(11)	2.070(2)
Ni(3)–N(2)	2.054(2)	Ni(3)–Cl(1)	2.404(1)
Ni(1)–O(4)–Ni(2)	112.06(9)	Ni(2)–Cl(1)–Ni(3)	87.72(3)
Ni(2)–N(5)–O(2)–Ni(1)	16.2(3)	Ni(2)–N(8)–O(3)–Ni(3)	20.9(3)
Ni(3)–N(11)–O(4)–Ni(1)	104.0(2)	Ni(3)–N(11)–O(4)–Ni(2)	27.1(2)

Each triangular Ni(1,2,3) subunit contains four pyridyloximate ligands that show three different coordination modes: one 1.011 ligand is coordinated to Ni(3), two oximate ligands in the 2.111 coordinative mode link Ni(1)/Ni(2) and Ni(2)/Ni(3) and finally one oximate in its 3.211 coordination mode acts as tridentate bridge between the three nickel atoms. Ni–O–N–Ni torsion angles are relatively low except for Ni(1)–O(4)–N(11)–Ni(3), which takes a value of 104.0(2)°. As consequence of the different ligands that define the sides of the triangular subunits the Ni(1)⋯Ni(2), Ni(1)⋯Ni(3), and Ni(2)⋯Ni(3) distances are 3.4583(5), 4.5577(6), and 3.3375(5) Å, respectively

The water molecules coordinated to the central Ni(1) generate a set of intramolecular H-bonds with the 1.011 pyridyloximate ligands (distance O(5)–H(SAO)⋯O(1) of 2.677(3) Å) and the chloride bridging atoms (distance O(5)–H(SBO)⋯Cl(1) of 3.090(3) Å). The pyridyl rings belonging to the oximate ligand N(8)–O(3) establish weak intermolecular π -stacking interactions (distance between centroids is 3.727 Å) with the pyridyl rings of the N(5)–O(2) oximate ligands.

$[\text{Ni}_5\text{Br}_3(\text{MeO})_4(\text{pyC}\{\text{CN}\}\text{NO})_3(\text{MeOH})_6] \cdot 1.5\text{MeOH} \cdot 0.5\text{H}_2\text{O}$ (**3**). Compound **3** can be described like a $\{\text{Ni}_4(\text{MeO})_4\}^{4+}$ cubane with an additional Ni^{II} ion linked to

one of its corners through three oximato bridges, as shown in Figure 3. Selected distances and angles for 3 are listed in Table

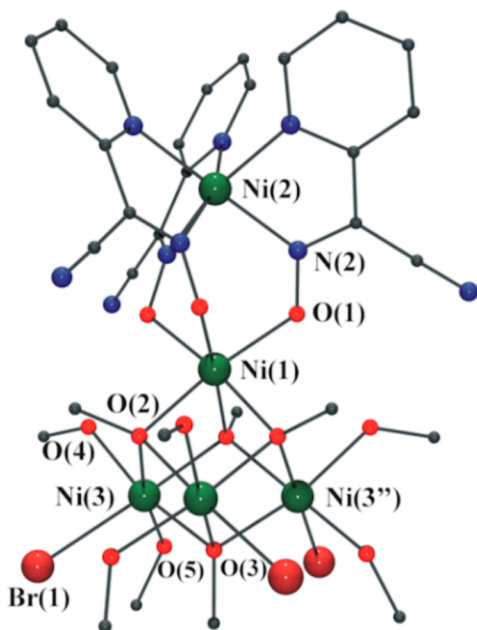


Figure 3. Partially labeled Pov-Ray plot of complex 3. All hydrogen atoms have been omitted for clarity.

Table 4. Selected Interatomic Distances (Å) and Angles (deg) for Compound 3

Ni(1)–O(1)	2.087(2)	Ni(1)–O(2)	2.050(2)
Ni(2)–N(1)	2.117(3)	Ni(1)–N(2)	2.044(4)
Ni(3)–Br(1)	2.587(1)	Ni(3)–O(3)	2.068(2)
Ni(3)–O(2)	2.050(2)	Ni(3)–O(4)	2.089(3)
Ni(3)–O(2')	2.075(2)	Ni(3)–O(5)	2.066(3)
Ni(1)–O(2)–Ni(3)	97.2(1)	Ni(3)–O(2)–Ni(3')	97.54(9)
Ni(1)–O(2)–Ni(3'')	96.45(9)	Ni(3)–O(3)–Ni(3')	97.2(1)
Ni(2)–N(2)–O(1)–Ni(1)	38.3(3)		

4. The external Ni(2) cation is coordinated to three pyridyloximate ligands by their six nitrogen atoms, exhibiting in consequence a NiN₆ environment. All three oximato bridges bind the same metallic center, Ni(1), that together with three μ₃-MeO[−] groups provide a NiO₆ environment. Remaining nickel atoms (Ni(3) and symmetry related) have a NiBrO₅ environment formed by three μ₃-MeO[−] groups, one bromide and two coordinated MeOH molecules. Bond angles in the cubane subunit show values in the short 96.5–97.5° range and Ni(1)–O(1)–N(2)–Ni(2) torsion angles are 38.3(3)°.

The methanol molecules coordinated to Ni(3) promote intramolecular H-bonds with the oximato ligands coordinated to Ni(2) with O(4)–H(4O)⋯O(1) distance of 2.760(4) Å and the bromine atoms with O(5)–H(5O)⋯Br(1) distance of 3.235(3) Å.

[Ni₅(OH)₂(pyC{CN}NO)₆(SCN)₂(H₂O)₃·5MeCN·4H₂O (4·5MeCN·4H₂O). The core of neutral complex 4 is depicted in Figure 4 and selected interatomic distances and angles are listed in Table 5. This compound can be described like a [Ni₃(μ₃–

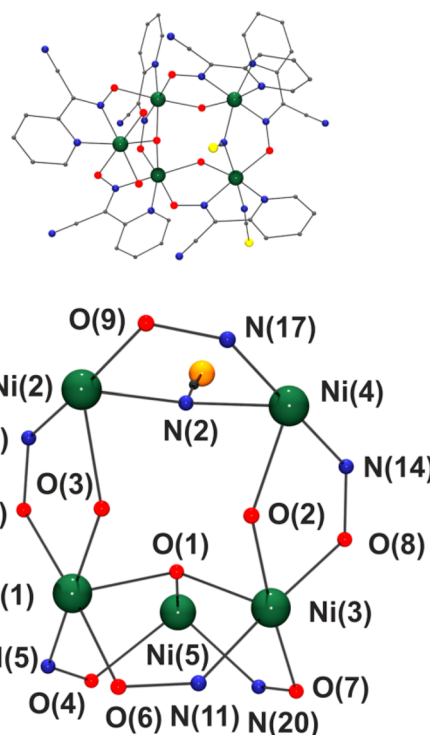


Figure 4. Partially labeled Pov-Ray plot of complex 4. All hydrogen atoms have been omitted for clarity. Compound 5 exhibits a similar structure with a methoxy bridge instead the thiocyanate ligand between Ni(2) and Ni(4).

Table 5. Selected Interatomic Distances (Å) and Angles (deg) for Compound 4

Ni(1)–N(3)	2.092(4)	Ni(1)–N(5)	2.041(4)
Ni(1)–O(1)	2.036(4)	Ni(1)–O(3)	2.075(3)
Ni(1)–O(5)	2.106(4)	Ni(1)–O(6)	2.067(4)
Ni(2)–N(1)	2.018(5)	Ni(2)–N(2)	2.121(4)
Ni(2)–N(6)	2.062(5)	Ni(2)–N(8)	2.066(4)
Ni(2)–O(3)	2.096(4)	Ni(2)–O(9)	2.047(3)
Ni(3)–N(9)	2.065(5)	Ni(3)–N(11)	2.048(5)
Ni(3)–O(1)	2.052(3)	Ni(3)–O(2)	2.055(3)
Ni(3)–O(7)	2.047(3)	Ni(3)–O(8)	2.069(4)
Ni(4)–N(12)	2.105(5)	Ni(4)–N(14)	2.053(4)
Ni(4)–N(15)	2.076(4)	Ni(4)–N(17)	2.039(4)
Ni(4)–N(2)	2.107(4)	Ni(4)–O(2)	2.027(4)
Ni(5)–N(18)	2.060(5)	Ni(5)–N(20)	2.049(5)
Ni(5)–O(1)	2.032(3)	Ni(5)–O(4)	2.050(4)
Ni(1)–O(3)–Ni(2)	114.8(2)	Ni(1)–O(1)–Ni(3)	111.9(2)
Ni(1)–O(1)–Ni(5)	112.4(2)	Ni(2)–N(2)–Ni(4)	109.7(2)
Ni(3)–O(2)–Ni(4)	115.8(2)	Ni(3)–O(1)–Ni(5)	112.7(2)
Ni(1)–N(5)–O(4)–Ni(5)	14.6(5)	Ni(2)–N(8)–O(5)–Ni(1)	0.5(5)
Ni(3)–N(11)–O(6)–Ni(1)	13.8(5)	Ni(4)–N(17)–O(9)–Ni(2)	12.1(5)
Ni(4)–N(14)–O(8)–Ni(3)	4.0(5)	Ni(5)–N(20)–O(7)–Ni(3)	2.5(5)

OH)(pyC{CN}NO)₃]²⁺ triangular fragment in which two Ni^{II} atoms are linked to a dinuclear subunit, providing the triangle a handle. The triangle binds the dinuclear subunit through two double oximato/aquo-hydroxo bridges (two hydroxo groups sharing one additional H atom by means of a strong H-bond, O(2)–H(2OB)⋯O(3) distance of 2.443(5) Å) and the Ni₂ subunit itself is linked by an oximato/thiocyanato bridge.

All three metal centers from the triangle, Ni(1), Ni(3), and Ni(5), have a NiN₂O₄ environment, while the remaining Ni(2) and Ni(4) present a NiN₄O₂ and NiN₅O environment, respectively. Ni(1) and Ni(3) bind one pyC{CN}NO[−] ligand by its two N atoms, the μ₃-OH group, one aquo-hydroxo bridge and two O-oximato bridges; Ni(5) is bound to one pyridyloximato ligand also by its two N atoms, to the μ₃-OH group, to one O-oximato bridge and finally to two coordinated water molecules. Ni(2) coordinates one pyC{CN}NO[−] ligand by the two N atoms, two thiocyanate ligands (one acting as a terminal group, the other one acting as an end-on bridging group), one aquo-hydroxo bridge, and two O-oximato bridges; and finally Ni(4) is tied to four N atoms from two different pyC{CN}NO[−] ligands, to the end-on bridging SCN[−] and to one aquo-hydroxo bridge.

The [Ni₃(μ₃-OH)(pyC{CN}NO)₃]²⁺ triangular fragment is roughly isosceles (Ni⋯Ni distances and Ni–O–Ni bond angles are comprised between 3.380 and 3.401 Å and 111.9–112.7°, respectively). The O-hydroxo atom is placed 0.577(3) Å out of the plane defined by the Ni(1,3,5) cations. The hydroxo and the N(2)-atom of the thiocyanate ligand establish an H-bond with O(1)–H(1O)⋯N(2) distance of 2.992(6) Å.

[Ni₅(MeO)₂(OH)_{1.5}(pyC{CN}NO)₆(H₂O)_{2.5}(MeOH)](NO₃)_{0.5}·2.75MeOH·1.25H₂O (5·2.75MeOH·1.25H₂O). Compound 5 presents a very similar core to 4, Figure 4. The main differences lie in the presence of a bridging methoxy group instead of the thiocyanate bridging ligand, the substitution of the terminal thiocyanate ligand by one methanol molecule and finally the coordinative change of the N(15)/N(17) containing pyridyloximato ligand from Ni(4) to Ni(2), so the O-oximato bridge now links Ni(4) instead of Ni(2). The charge difference generated by the substitution of the anionic SCN[−] ligand by the neutral methanol group is compensated with an aquo/hydroxo group with a 50% occupancy and the anionic nitrate, also exhibiting a 50% occupancy.

Further structural details of 5 are not mentioned to avoid repetitive descriptions. Table 6 lists selected interatomic distances and angles for 5.

Comments on the Ni₅ Topologies. In this work, we have presented five new complexes from the Ni₅/2-pyridyloxime system. Considering the complexes reported in this work and those previously reported, there are a total of 14 Ni₅/2-pyridyloximato complexes which surprisingly exhibit up to 8 different topologies, Scheme 2.

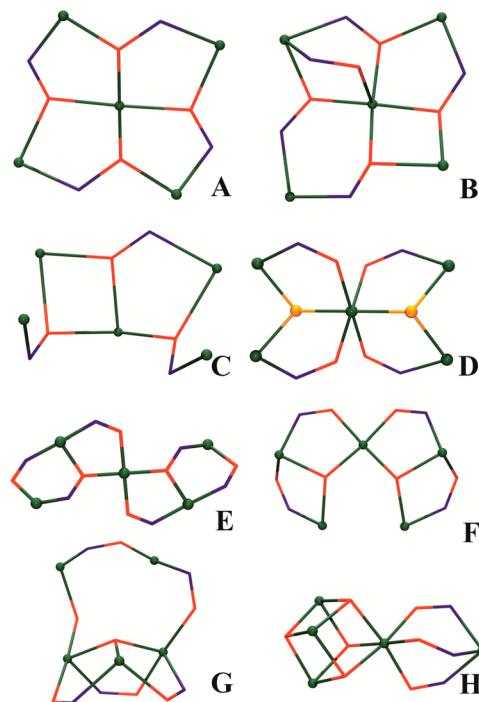
In the search for a relationship between reactants (mainly the 2-pyridyloxime ligand and the Ni^{II} counteranions) and the resulting topologies, some trends can be drawn: (i) 4-Hydroxysalicylhydroxamate leads to stabilize 12-MC cyclic molecules in which the metallacrown is formed by four metallic centers linked through four oximato bridges that generate a {–M–N–O–}₄ ring. These rings are able to coordinate a fifth central metallic cation employing the O-oximato atoms, Scheme 2A, as has been observed in Cu,²⁰ Mn²¹, and heterometallic chemistry.²² Similar centered metallacrowns were obtained when using the rigid Indane-1,2,3-trione-trioxime or Indane-1,2,3-trione-dioxime ligands. The stability of these metallacrowns arises from the bridges provided by the presence of an extra O-donor atom from the hydroxo groups located near the C-oximato atom.²³

When 4-hydroxysalicylhydroxamate was combined with di-2-pyridyloxime (py₂CNOH), a similar centered Ni₄-metallacrown,¹⁹ Scheme 2A, was obtained. In this case, the complex contains two salicyl and two pyridyloximates and the second N-

Table 6. Selected Interatomic Distances (Å) and Angles (deg) for Compound 5

Ni(1)–N(3)	2.112(4)	Ni(1)–N(5)	2.042(4)
Ni(1)–O(1)	2.043(3)	Ni(1)–O(3)	2.049(3)
Ni(1)–O(5)	2.109(4)	Ni(1)–O(6)	2.068(4)
Ni(2)–N(6)	2.097(4)	Ni(2)–N(8)	2.044(4)
Ni(2)–N(15)	2.122(4)	Ni(2)–N(17)	2.049(4)
Ni(2)–O(3)	2.078(4)	Ni(2)–O(12)	2.009(3)
Ni(3)–N(9)	2.066(5)	Ni(3)–N(11)	2.053(4)
Ni(3)–O(1)	2.049(3)	Ni(3)–O(2)	2.121(4)
Ni(3)–O(7)	2.060(4)	Ni(3)–O(8)	2.069(4)
Ni(4)–N(12)	2.059(5)	Ni(4)–N(14)	2.032(5)
Ni(4)–O(2)	2.089(4)	Ni(4)–O(9)	2.032(4)
Ni(4)–O(12)	2.038(3)	Ni(4)–O(13)	2.105(4)
Ni(5)–N(18)	2.076(4)	Ni(5)–N(20)	2.032(4)
Ni(5)–O(1)	2.036(3)	Ni(5)–O(4)	2.088(4)
Ni(1)–O(3)–Ni(2)	113.3(2)	Ni(1)–O(1)–Ni(3)	110.9(2)
Ni(1)–O(1)–Ni(5)	112.1(2)	Ni(2)–O(12)–Ni(4)	111.1(2)
Ni(3)–O(2)–Ni(4)	111.5(2)	Ni(3)–O(1)–Ni(5)	111.3(2)
Ni(1)–N(5)–O(4)–Ni(5)	14.5(4)	Ni(2)–N(8)–O(5)–Ni(1)	7.1(4)
Ni(2)–N(17)–O(9)–Ni(4)	16.5(4)	Ni(3)–N(11)–O(6)–Ni(1)	10.6(4)
Ni(4)–N(14)–O(8)–Ni(3)	0.8(5)	Ni(5)–N(20)–O(7)–Ni(3)	9.1(4)

Scheme 2. Pov-Ray Plot of the Cores of the Different Topologies for the Ni₅/2-Pyridyloximes System^a



^aNi atoms are plotted in green, nitrogen in blue, oxygen in red, and orange atoms in topology D can be oxygen or N-azide atoms.

pyridyl donor of the py₂CNO[−] ligand plays the same role than the hydroxo group of the 4-hydroxysalicylhydroxamate, helping to stabilize the macrocyclic arrangement.

Reaction of py₂CNOH ligand with nickel nitrate leads to a similar metallacrown^{8h} but with an extra oximato bond between the metallacrown and the central Ni^{II} cation, Scheme 2B. In this

case, all the bridges were provided by the oximate groups and the additional coordination of the second N-pyridyl donor.

(ii) The reaction of py_2CNOH ligand in acetone/aqueous medium with nickel acetate generates an irregular core Scheme 2C, formed by only three 3.2110 or 3.2111 oximates and six carboxylate bridges.^{8c} In this case, most of the coordination sites of the Ni^{II} cations are occupied by O-carboxylate bridges avoiding the coordination of the secondary N-pyridyl donor atoms and so the metallacrown is no longer formed.

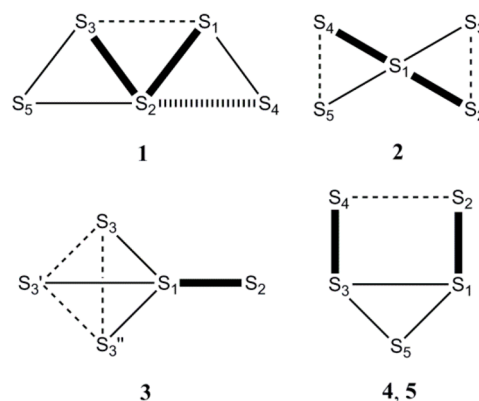
(iii) The use of 2-pyridyloxime ligands in presence of carboxylic groups mainly generates bowtie cores,^{8b,d,f,24} as diacetylpyridyldioxime (dapdoH_2), phenyl-2-pyridyloxime ($\{\text{ph}\}\{\text{py}\}\text{CNOH}$), 6-methyl-2-pyridyloxime (6-MepyCNOH), and 2-pyridylcyanoxime ($\text{pyC}\{\text{CN}\}\text{NOH}$) ligands have proved. All these clusters can be separated into two main groups: μ_3 -OR or $\mu_3\text{-N}_3$ centered triangles, Scheme 2D and O-oximate centered ones, in which the oximate ligand itself binds the triangles from the outside and the inside, Scheme 2E. The presence of squareplanar Ni(II) ions or the absence of available OH^- and N_3^- ligands cause the 2-E type of bowtie cores instead 2-D.

(iv) Finally, three new topologies have been shown in this Article: In the first place, coordination of the highly hindered $\text{Ph}_2\text{CHCOO}^-$ carboxylate ligands yields a distorted trapezium, Scheme 2F. In second place, the reaction of inorganic nickel salts (thiocyanate or nitrate in methanolic medium) leads to additional thiocyanate or methoxide bridges, resulting in two triangles with a Ni_2 grip or handle, Scheme 2G. In the last place, a new and surprising $\text{Ni}_4(\text{MeO})_4$ cubane coordinated by three oximate bridges to an extra Ni^{2+} ion has been discovered, Scheme 2H, when the reaction was set with $\text{pyC}\{\text{CN}\}\text{NOH}$ and NiBr_2 .

Despite that the relationship between the reactants and the resulting topology is highly serendipitous it could be pointed out that topologies 2-A and -B are dependent on additional O,N-donor groups attached to the vicinity of the oximate groups, which provide additional bridges in the adequate direction and that the most common structure 2-D, is related to the presence of carboxylate counteranions. The effect of the solvent is difficult to predict but in some cases the resulting product can be justified a posteriori: as example the reaction starting from nickel halides yields topology 2-E employing a coordinating solvent as methanol, whereas topology 2-H was obtained when the solvent (CH_2Cl_2) is unable to link the nickel cations. Oximate, carboxylate and alcoxyl/hydroxo bridges induce typically antiferromagnetic interactions and low spin ground states are usually found for all the analyzed topologies, being $S = 1$ the expected ground state. Interestingly, competitive interactions can lead to diamagnetic $S = 0$ ground states despite the odd number of paramagnetic centers as will be further discussed. Larger spin states, up to the maximum $S = 5$, have been reported only for the 2-D bowtie topology when additional $\mu_3\text{-1,1,1}$ azido bridges are involved in the center of the shared triangles.

Magnetic Measurements and Modeling. The numbering of all the spin carriers in the Hamiltonians applied to 1–5 and in the subsequent discussion is provided in Scheme 3. The fit of the experimental data was made using CLUMAG program²⁵ for all complexes and applying the Hamiltonians derived from the corresponding interaction scheme. The number of coupling constants for each topology has been minimized as possible in basis to structural considerations to avoid overparametrization.

Scheme 3. Schematic of the Magnetic Interactions for 1–5 (See Text for the Corresponding Hamiltonians)



The room temperature $\chi_M T$ value for 1 is $4.96 \text{ cm}^3 \text{ K mol}^{-1}$, which on cooling decreases continuously down to $0.75 \text{ cm}^3 \text{ K mol}^{-1}$ at 2 K, Figure 5. The complex has seven interaction

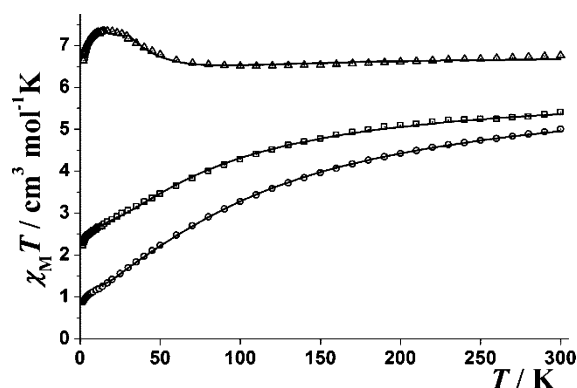


Figure 5. Product of $\chi_M T$ vs T for compounds 1 (dot centered circles), 2 (dot centered squares), and 3 (triangles). Solid lines show best obtained fit.

pathways but the number superexchange pathways can be reduced attending to the kind of bridges: double oxo bridge (J_1), double hydroxo/oximate (J_2), triple hydroxo/oximate/carboxylate (J_3), and single hydroxo bridge (J_4). The 4- J Hamiltonian was

$$H = -J_1(S_1 \cdot S_3) - J_2(S_2 \cdot S_4) - J_3(S_2 \cdot S_5 + S_1 \cdot S_4 + S_3 \cdot S_5) - J_4(S_1 \cdot S_2 + S_2 \cdot S_3)$$

The best fit parameters were $J_1 = +5.9 \text{ cm}^{-1}$, $J_2 = -29.0 \text{ cm}^{-1}$, $J_3 = -22.0 \text{ cm}^{-1}$, $J_4 = -12.9 \text{ cm}^{-1}$, and $g = 2.14$, with $R = 1.75 \times 10^{-5}$ ($R = (\chi_M T_{\text{exp}} - \chi_M T_{\text{calcd}})^2 / (\chi_M T_{\text{exp}})^2$). Calculation of the energy of the lower spin states indicates an $S = 1$ ground state followed by one $S = 0$ with a gap of 10.6 cm^{-1} and well isolated of larger spin states (the gap with the nearest $S = 2$ level is 26.0 cm^{-1}). Magnetization experiments show a nonsaturated value equivalent to 1.8 electrons, consistent with the population of the $S = 1$ ground state and a partial population of the low-lying $S = 0$ level.

Compound 2 presents a room temperature $\chi_M T$ value of $5.40 \text{ cm}^3 \text{ K mol}^{-1}$ that drops when cooling down to $2.23 \text{ cm}^3 \text{ K mol}^{-1}$ at 2 K, Figure 5. In this case there are three very different superexchange pathways and thus the applied Hamiltonian for the centrosymmetric compound 2 is

$$H = -J_1(S_1 \cdot S_2 + S_1 \cdot S_4) - J_2(S_1 \cdot S_3 + S_1 \cdot S_5) \\ - J_3(S_2 \cdot S_3 + S_4 \cdot S_5)$$

Best fit parameters were $J_1 = -19.8 \text{ cm}^{-1}$, $J_2 = -16.6 \text{ cm}^{-1}$, $J_3 = -12.3 \text{ cm}^{-1}$, and $g = 2.20$, with $R = 3.36 \times 10^{-5}$. Calculation of the energy of the lower spin states indicates an $S = 1$ ground state, but in this case, quasi degenerate with an $S = 0$ and two $S = 2$ spin levels. Effective population of the ground state only is possible below 2 K, explaining the shape and value of the lower $\chi_M T$ experimental plot and its value of $2.23 \text{ cm}^3 \text{ K mol}^{-1}$ at 2 K. In good agreement, magnetization plot tends to the equivalent value of 3.5 electrons as result of the partial population of the low lying $S = 2$ spin levels at this temperature.

The $\chi_M T$ product at room temperature for compound **3** is $6.76 \text{ cm}^3 \text{ K mol}^{-1}$ and then the curve diminishes to $6.52 \text{ cm}^3 \text{ K mol}^{-1}$ at 100 K. Below this minimum the plot increases up to a maximum $\chi_M T$ value of $7.34 \text{ cm}^3 \text{ K mol}^{-1}$ at 17 K suggesting a ferrimagnetic response with predominant ferromagnetic coupling. Finally, at lower temperatures, the $\chi_M T$ value decreases and reaches $6.64 \text{ cm}^3 \text{ K mol}^{-1}$ at 2 K, due to ZFS or weak intercluster interactions, Figure 5.

Complex **3** clearly shows three different interaction pathways and on basis on the structural parameters the experimental data were fitted (in the 300–30 K temperature range) with the 3- J Hamiltonian:

$$H = -J_1(S_1 \cdot S_2) - J_2(S_1 \cdot S_3 + S_1 \cdot S_3' + S_1 \cdot S_{3''}) \\ - J_3(S_3 \cdot S_3' + S_3 \cdot S_{3''} + S_3' \cdot S_{3''})$$

Best parameters obtained were $J_1 = -51.4 \text{ cm}^{-1}$, $J_2 = +3.9 \text{ cm}^{-1}$, $J_3 = +11.0 \text{ cm}^{-1}$, and $g = 2.32$, with $R = 4.10 \times 10^{-5}$. Fit values justify the ferrimagnetic response of **3**, pointed out by the minimum in the $\chi_M T$ plot: between room temperature and 100 K the dominant interaction corresponds to the strong antiferromagnetic interaction mediated by J_1 whereas at lower temperatures the ferromagnetic interactions inside the cubane fragment increase the $\chi_M T$ value, resulting in an $S = 3$ ground state. The magnetization plot shows a quasi saturated value of $6.5 \mu_B$ at 5 T, that arises from the population of the well isolated $S = 3$ ground state.

$\chi_M T$ product versus T for compounds **4** and **5** are depicted in Figure 6. Room temperature $\chi_M T$ value for **4** is $5.00 \text{ cm}^3 \text{ K mol}^{-1}$ and decreases on cooling down to $0.88 \text{ cm}^3 \text{ K mol}^{-1}$ at 2 K. Compound **5** shows a $\chi_M T$ value of $4.36 \text{ cm}^3 \text{ K mol}^{-1}$ at 300

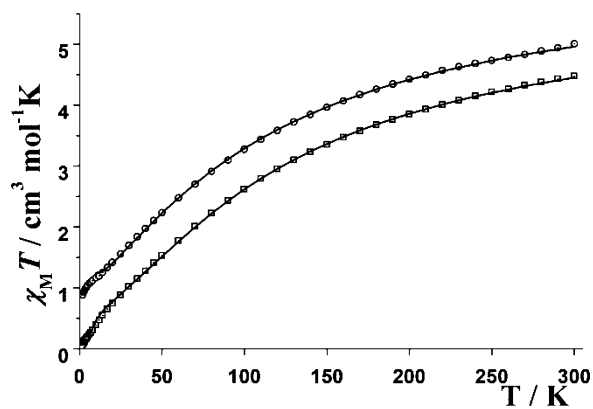


Figure 6. Product of $\chi_M T$ vs T for compounds **4** (dot centered circles) and **5** (dot centered squares). Solid lines show best obtained fit.

K and surprisingly, tends to zero at low temperature and the χ_M plot exhibit a well-defined maximum at 11 K.

As was pointed out in the structural description, Ni–O–Ni and Ni–O–N–Ni angles inside the μ_3 -OH centered triangle Ni(1,3,5) are practically identical and thus these three interactions were joined as J_1 . By the same reasons the interaction between Ni(1)/Ni(2) and Ni(3)/Ni(4) were joined in a common J_2 coupling constant. The interaction between Ni(2) and Ni(4) corresponds to a very different pathway for each compound: in **4** is a double oximate/ $\mu_{1,1}$ -NCS bridge whereas for **5** is a double oximate/alkoxo bridge. The corresponding 3- J Hamiltonian is

$$H = -J_1(S_1 \cdot S_5 + S_3 \cdot S_5 + S_1 \cdot S_3) - J_2(S_1 \cdot S_2 + S_3 \cdot S_4) \\ - J_3(S_2 \cdot S_4)$$

The best obtained fit corresponds to $J_1 = -37.6 \text{ cm}^{-1}$, $J_2 = -41.4 \text{ cm}^{-1}$, $J_3 = -0.7 \text{ cm}^{-1}$, and $g = 2.23$, with $R = 3.78 \times 10^{-5}$ for **4** and $J_1 = -39.6 \text{ cm}^{-1}$, $J_2 = -40.4 \text{ cm}^{-1}$, $J_3 = -35.9 \text{ cm}^{-1}$ and $g = 2.19$, with $R = 2.91 \times 10^{-4}$ for **5** (in the range of 300–10 and 300–2 K, respectively). From these data, a simplified fit assuming $J_1 = J_2 \neq J_3$ for **4** and $J_1 = J_2 = J_3$ for **5** gives average values of $J_1 = J_2 = -41.4 \text{ cm}^{-1}$, $J_3 = -1.6 \text{ cm}^{-1}$, and $g = 2.27$ for **4** and $J_1 = J_2 = J_3 = -37.2 \text{ cm}^{-1}$, and $g = 2.17$ for **5** with a similar quality. As could be expected from structural data, J_1 and J_2 take similar values in the two compounds. It should be pointed out that the value of J_3 is poorly reliable for compound **4**: its low value in comparison with the strong coupling mediated by J_1 and J_2 do not influence the shape of the plot as was checked fixing its value in the $\pm 5 \text{ cm}^{-1}$ range. Thus, for the interaction mediated by the double oximate/thiocyanate bridges we are only able to propose a non quantified very weak magnetic interaction, probably antiferromagnetic. Magnetization plot for **4** shows a nonsaturated value equivalent to 1.8 electrons under the maximum applied field of 5 T. In contrast, no magnetization was obtained for compound **5** in agreement with the overall antiferromagnetic coupling.

Magnetic properties of complexes **4** and **5** become unusual and the different low-temperature response is not evident for this new Ni₅ topology. To justify the $S = 1$ (for **4**) and $S = 0$ (for **5**) ground states suggested by the susceptibility measurements we performed a more detailed analysis of the energy dependence of the low energy spin levels as function of the coupling constants.

According to the obtained fit values, the main difference among **4** and **5** lies in the very different value of J_3 : for complex **4** J_1 and J_2 have similar values but $J_1 \approx J_2 \gg J_3$ and the ground state is apparently $S = 1$ whereas for complex **5** the three constants have similar values ($J_1 \approx J_2 \approx J_3$) and the ground state is clearly $S = 0$. Thus, it appears an evident relationship between J_3 and the stabilization of the diamagnetic ground state and to analyze this effect, the system was modeled as is shown in the coupling scheme plotted in Figure 7 (right), assuming $J_A = J_1 = J_2$ and $J_B = J_3$. Thus the analyzed Hamiltonian was

$$H = -J_A(S_1 \cdot S_5 + S_3 \cdot S_5 + S_1 \cdot S_3 + S_1 \cdot S_2 + S_3 \cdot S_4) \\ - J_B(S_2 \cdot S_4)$$

The J_A value was fixed to -40 cm^{-1} (close to the fit value of J_1 and J_2) and J_B was systematically explored between 0 and -40 cm^{-1} range of values. The energy for the low lying spin levels $S = 0, 1$, and 2 are plotted in Figure 7 right, as function of the J_B/J_A ratio. Analysis of this plot shows that $S = 0$ is the

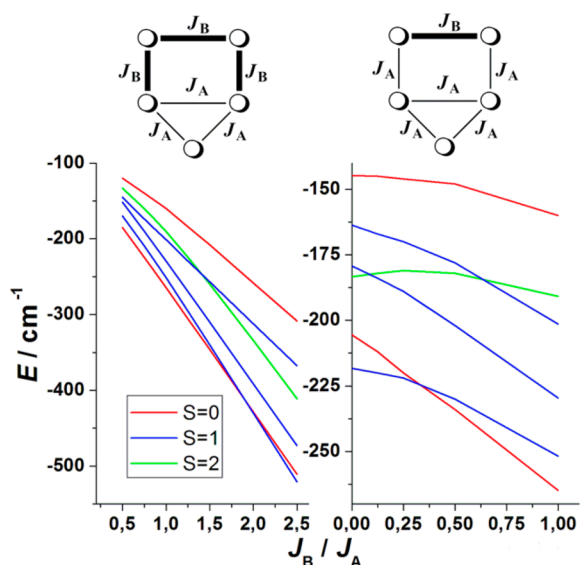


Figure 7. Coupling scheme and plot of energy of the low-lying spin levels for the optimized triangle-with-handle topology (left) and for complexes **4** and **5** (right). The values for $J_B/J_A = 1$ are a common point in both plots.

ground state for larger J_B/J_A ratios. In contrast, for lower J_B/J_A ratios one well isolated $S = 1$ becomes the ground state, being the frustration point at $J_B/J_A = 1/3$.

For **4**, the calculated value of J_3 leads to one J_B/J_A ratio on the lower limit of the plot with its associated $S = 1$ ground state. At low temperature, both spin levels are populated explaining the intermediate value of $0.88 \text{ cm}^3 \text{ K mol}^{-1}$ at 2 K and the low and nonsaturated value of magnetization.

For **5**, the calculated value of J_3 is similar to J_1 and J_2 (J_B is similar to J_A) and the J_B/J_A ratio is close to 0.9. This J_B/J_A ratio leads to an $S = 0$ ground state that confirms the quasi-diamagnetic behavior observed in the magnetization measurement at 2 K. In simple terms, complex **5** can be envisaged as an equilateral triangle antiferromagnetically coupled (local $S = 0$) and a dimeric unit also antiferromagnetically coupled.

The topology of compounds **4** and **5** consists of a nearly equilateral triangle sharing one of its sides with a square arrangement of spin carriers (triangle-with-handle). To check if the diamagnetic ground state is inherent to this topology or if it could be dependent on the relative strength of the interactions inside each fragment, a new simulation was performed in order to give a wide characterization of this unusual Ni_5 arrangement.

Thus, the system was modeled according the coupling scheme plotted in Figure 7 left with the Hamiltonian:

$$H = -J_A(S_1 \cdot S_5 + S_3 \cdot S_5 + S_1 \cdot S_3) - J_B(S_1 \cdot S_2 + S_3 \cdot S_4 + S_2 \cdot S_4)$$

As in the above case, the J_A value was fixed to -40 cm^{-1} (close to the fit values of J_1) and J_B was systematically explored between -20 and -100 cm^{-1} range of values. Figure 7 left shows the energy trends for the low lying spin levels $S = 0, 1$, and 2 as function of the J_B/J_A ratio for triangle-with-handle compounds in which $J_A = J_1 \neq J_B = J_2 = J_3$.

Analysis of this plot shows how for the larger J_B/J_A ratios the ground state is $S = 0$, well isolated from the nearest $S = 1$ spin level. In contrast, for lower J_B/J_A ratios $S = 1$ becomes the ground state but relatively close to the $S = 0$ with the frustration

point placed at $J_B/J_A = 2.0$. In short, the ground state is function of the relative strength of the antiferromagnetic interaction inside the triangle and the handle and for similar interactions (as occurs in compound **5**, $S = 0$ should be expected).

Magnetic Correlations. DFT calculations previously reported by the authors,^{8b,10} have shown that the antiferromagnetic interaction inside triangular $[\text{Ni}_3(\mu_3\text{-OH})(\text{R-NO})_3]^{2+}$ fragments is strongly dependent on the Ni–O–Ni bond angle involving the central $\mu_3\text{-OH}$ bridge. All the hydroxo/oximate mediated coupling constants reported in this paper present J values that lie in the calculated range (between -15 and -50 cm^{-1}) and the values around -40 cm^{-1} for the triangular subunits of **4** and **5** with Ni–O–Ni bond angles in the short $110.9\text{--}112.7$ range of values are fully consistent with the correlations and the recently reported $[\text{Ni}_3(\mu_3\text{-OH})(\text{R-NO})_3]^{2+}$ triangles.¹⁰ In the same way, the antiferromagnetic coupling associated to hydroxo/oximate bridges with lower Ni–O–Ni bond angles present in compound **1** show weaker antiferromagnetic interaction ($J_2 = 29.0 \text{ cm}^{-1}$ and $J_3 = 22.0 \text{ cm}^{-1}$) in good agreement with the expected values, providing additional proofs of the validity of the proposed model. Ni–O–Ni and Ni–O–O–N–Ni bond and torsion angles involved in these superexchange pathways are very similar and thus, the lower value obtained for J_3 should be related with the anticomplementary interaction of the syn–syn carboxylate bridge.

The oximate/pseudohalide bridges have been characterized only for the oximate/ $\mu_{1,1}\text{-N}_3$ case for which we proved its moderate ferromagnetic response.^{8e} Compound **4** gives the first example of oximate/N-thiocyanate double bridge. Magnetically, this double bridge behaves different of the azido case showing a weak and probably antiferromagnetic response.

Finally, it should be pointed out that the series of topologies reported for the $\text{Ni}_5/\text{oximate}$ system tends to give low S ground states, mainly $S = 0$ and 1 , as corresponds with the oximate or oximate/hydroxo bridges that give moderate or strong antiferromagnetic interactions. The combination of oximates with $\mu_{1,1}\text{-N}_3$ or $\mu_{1,1,1}\text{-N}_3$ (bowtie topology D, Scheme 2), gives the unique examples in which the maximum $S = 5$ ground state has been reached, arising as the best combination of ligands to obtain large spins that could lead to SMM response.

CONCLUSIONS

The employment of 2-pyridylcyanoxime ligand with different carboxylate and noncarboxylate Ni^{2+} salts has led to five new $\text{Ni}_5/2\text{-pyridylloxime}$ clusters. These new complexes provided three new topologies together with the first example of the oximate/N-thiocyanate double bridge.

Magnetic measurements were carried in the $300\text{--}2 \text{ K}$ range and revealed antiferromagnetic response for **1**, **2**, **4**, and **5** and ferrimagnetic behavior for **3**. All OH/oximate mediated magnetic interactions present coupling constant values that agree with the expected ones from previous DFT calculations. The oximate/N-thiocyanate double bridge proves to be a poorly efficient superexchange pathway in contrast with the clearly ferromagnetic character of the oximate/ $\mu_{1,1}\text{-N}_3$ case.

Analysis of this system is an excellent example for serendipitous assembly: among the 14 $\text{Ni}_5/2\text{-pyridylloxime}$ clusters that have been characterized, 8 different topologies have been observed and only for three of them an approach to rational design could be suggested. These variations come from small changes in the ligand (substitution on the vicinal C-atom to the oximate function), solvent coordination and the counteranion of the starting Ni^{II} salt.

■ ASSOCIATED CONTENT

Supporting Information

Crystallographic data in CIF format for compounds 1–5. This material is available free of charge via the Internet at <http://pubs.acs.org>.

■ AUTHOR INFORMATION

Corresponding Authors

*E-mail: jordi.esteban@qi.ub.edu.

*E-mail: albert.escuer@ub.edu.

Present Address

[†]José Sánchez Costa: LCC, CNRS, and Université de Toulouse (UPS, INP), 205 route de Narbonne, 31077, Toulouse, France.

Author Contributions

The manuscript was written through contributions of all authors.

Notes

The authors declare no competing financial interest.

■ ACKNOWLEDGMENTS

Funds from CICYT Project CTQ2012-30662 are acknowledged. A.E. is thankful for financial support from the Excellence in Research ICREA-Academia Award. The Advanced Light Source is supported by the Director, Office of Science, Office of Basic Energy Sciences, of the U.S. Department of Energy under Contract No. DE-AC02-05CH11231.

■ REFERENCES

- (1) (a) Rosa, D. T.; Krause Bauer, J. A.; Baldwin, M. J. *Inorg. Chem.* **2001**, *40*, 1606. (b) Akine, S.; Taniguchi, T.; Saiki, T.; Nabeshima, T. *J. Am. Chem. Soc.* **2005**, *127*, 540. (c) Goldcamp, M. J.; Robison, S. E.; Krause Bauer, J. A.; Baldwin, M. J. *Inorg. Chem.* **2002**, *41*, 2307.
- (2) (a) Boyd, P. D. W.; Li, Q.; Vincent, J. B.; Folting, K.; Chang, H. R.; Streib, W. E.; Huffman, J. C.; Christou, G.; Hendrickson, D. N. *J. Am. Chem. Soc.* **1988**, *110*, 8537. (b) Milios, C. J.; Inglis, R.; Vinslava, A.; Bagai, R.; Wernsdorfer, W.; Parsons, S.; Perlepes, S. P.; Christou, G.; Brechin, E. K. *J. Am. Chem. Soc.* **2007**, *129*, 12505. (c) Choi, H. J.; Sokol, J. J.; Long, J. R. *Inorg. Chem.* **2004**, *43*, 1606. (d) Bogani, L.; Wernsdorfer, W. *Nat. Mater.* **2008**, *7*, 179. (e) Aromi, G.; Parsons, S.; Wernsdorfer, W.; Brechin, E. K.; McInnes, E. J. L. *Chem. Commun.* **2005**, 5038.
- (3) (a) Dietrich, B.; Guilhem, J.; Lehn, J. M.; Pascard, C.; Sonveaux, E. *Helv. Chim. Acta* **1984**, *67*, 91. (b) Ulrich, S.; Petitjean, A.; Lehn, J. M. *Eur. J. Inorg. Chem.* **2010**, 1913.
- (4) (a) Yoneya, M.; Yamaguchi, T.; Sato, S.; Fujita, M. *J. Am. Chem. Soc.* **2012**, *134*, 14401. (b) Fujita, D.; Suzuki, K.; Sato, S.; Yagi-Utsumi, M.; Yamaguchi, Y.; Mizuno, N.; Kumasaka, T.; Takata, M.; Noda, M.; Uchiyama, S.; Kato, K.; Fujita, M. *Nat. Commun.* **2012**, *3*, 1093.
- (5) (a) Biros, S. M.; Yeh, R. M.; Raymond, K. N. *Angew. Chem., Int. Ed.* **2008**, *47*, 6062. (b) Brown, C. J.; Miller, G. M.; Johnson, M. W.; Bergman, R. G.; Raymond, K. N. *J. Am. Chem. Soc.* **2011**, *133*, 11964.
- (6) (a) Winpenny, R. E. P. *J. Chem. Soc., Dalton Trans.* **2002**, 1. (b) Aromi, G.; Bell, A. R.; Helliwell, M.; Raftery, J.; Teat, S. J.; Timco, G. A.; Roubeau, O.; Winpenny, R. E. P. *Chem.—Eur. J.* **2003**, *9*, 3024. (c) Mukherjee, P.; Mukherjee, S. *Acc. Chem. Res.* **2013**, *46* (11), 2556 DOI: 10.1021/ar400059q.
- (7) Milios, C. J.; Stamatatos, T. C.; Perlepes, S. P. *Polyhedron* **2006**, *25*, 134.
- (8) (a) Escuer, A.; Esteban, J.; Aliaga-Alcalde, N.; Font-Bardia, M.; Calvet, T.; Roubeau, O.; Teat, S. J. *Inorg. Chem.* **2010**, *49*, 2259. (b) Esteban, J.; Ruiz, E.; Font-Bardia, M.; Calvet, T.; Escuer, A. *Chem.—Eur. J.* **2012**, *18*, 3637. (c) Stamatatos, T. C.; Diamantopoulou, E.; Raptopoulou, C. P.; Psycharis, V.; Escuer, A.; Perlepes, S. P. *Inorg. Chem.* **2007**, *46*, 2350. (d) Escuer, A.; Esteban, J.; Roubeau, O. *Inorg. Chem.* **2011**, *50*, 8893. (e) Escuer, A.; Esteban, J.; Font-Bardia, M. *Chem. Commun.* **2012**, 48, 9777. (f) Esteban, J.; Font-Bardia, M.; Escuer, A. *Inorg. Chem.* **2014**, *53*, 1113. (g) Stamatatos, T. C.; Abboud, K. A.; Perlepes, S. P.; Christou, G. *Dalton Trans.* **2007**, 3861. (h) Stamatatos, T. C.; Escuer, A.; Abboud, K. A.; Raptopoulou, C. P.; Perlepes, S. P.; Christou, G. *Inorg. Chem.* **2008**, *47*, 11825. (i) Esteban, J.; Alcázar, L.; Torres-Molina, M.; Monfort, M.; Font-Bardia, M.; Escuer, A. *Inorg. Chem.* **2012**, *51*, 5503.
- (9) Escuer, A.; Vlahopoulou, G.; Perlepes, S. P.; Mautner, F. A. *Inorg. Chem.* **2011**, *50*, 2468.
- (10) (a) Esteban, J.; Font-Bardia, M.; Escuer, A. *Eur. J. Inorg. Chem.* **2013**, 5274. (b) Esteban, J.; Font-Bardia, M.; Escuer, A. *Inorg. Chem. Commun.* **2014**, DOI: 10.1016/j.inoche.2014.02.033.
- (11) Alcazar, L.; Cordero, B.; Esteban, J.; Tangoulis, V.; Font-Bardia, M.; Calvet, T.; Escuer, A. *Dalton Trans.* **2013**, 42, 12334.
- (12) Coxall, R. A.; Harris, S. G.; Henderson, D. K.; Parsons, S.; Tasker, P. A.; Winpenny, R. E. P. *Chem. Soc., Dalton Trans.* **2000**, 2349.
- (13) (a) Gerasimchuk, N. N.; Skopenko, V. V.; Domasevich, K. V.; Zhmurko, O. A. *Ukr. Khim. Zh. (Russ. Ed.)* **1992**, *58*, 935. (b) Mokhir, A. A.; Domasevich, K. V.; Dalley, N. K.; Kou, X.; Gerasimchuk, N. N.; Gerasimchuk, O. A. *Inorg. Chim. Acta* **1999**, *284*, 85.
- (14) Sheldrick, G. M. *SHELXS—A Computer Program for Determination of Crystal Structures*; University of Göttingen: Göttingen, Germany, 1997.
- (15) Sheldrick, G. M. *SHELX97—A Program for Crystal Structure Refinement*; University of Göttingen: Göttingen, Germany, 1997.
- (16) *International Tables of X-Ray Crystallography*, Vol. IV; Kynoch Press: Witton, Birmingham, U.K., 1974, 99–100 and 149.
- (17) Ortep-3 for Windows; Farrugia, L. J. *J. Appl. Crystallogr.* **1997**, *30*, 565.
- (18) (a) Davies, W. C.; Evans, G. B.; Hulbert, F. L. *J. Chem. Soc.* **1939**, 412. (b) Alcazar, L.; Cordero, B.; Esteban, J.; Tangoulis, V.; Font-Bardia, M.; Calvet, T.; Escuer, A. *Dalton Trans.* **2013**, 42, 12334. (c) Lampropoulos, C.; Abboud, K. A.; Stamatatos, T. C.; Christou, G. *Inorg. Chem.* **2009**, *48*, 813.
- (19) Psomas, G.; Stemmler, A. J.; Dendrinou-Samara, C.; Bodwin, J. J.; Schneider, M.; Alexiou, M.; Kanpf, J. W.; Kessissoglou, D. P.; Pecoraro, V. L. *Inorg. Chem.* **2001**, *40*, 1562.
- (20) Herring, J.; Zeller, M.; Zaleski, C. M. *Acta Crystallogr.* **2011**, *E67*, m41.
- (21) (a) Lah, M. S.; Pecoraro, V. L. *J. Am. Chem. Soc.* **1989**, *111*, 7258. (b) Dendrinou-Samara, C.; Papadopoulos, A. N.; Malamatri, D. A.; Tarushi, A.; Raptopoulou, C. P.; Terzis, J.; Samaras, E.; Kessissoglou, D. P. *J. Inorg. Biochem.* **2005**, *99*, 864.
- (22) Mezei, G.; Zaleski, C. M.; Pecoraro, V. L. *Chem. Rev.* **2007**, *107*, 4933.
- (23) Che, Z.; Jia, M.; Zhang, Z.; Liang, F. *Cryst. Growth Des.* **2010**, *10*, 4807.
- (24) (a) Papatriantafyllopoulou, C.; Stamatatos, T. C.; Wernsdorfer, W.; Teat, S. J.; Tasiopoulos, A. J.; Escuer, A.; Perlepes, S. P. *Inorg. Chem.* **2010**, *49*, 10486. (b) Escuer, A.; Vlahopoulou, G.; Mautner, F. A. *Dalton Trans.* **2011**, 40, 10109.
- (25) Gatteschi, D.; Pardi, L. *Gazz. Chim. Ital.* **1993**, *123*, 231.